

## **Reduced Cost of Reactive Power in Doubly Fed Induction Generator Wind Turbine System With Optimized Grid Filter**

Zhou, Dao; Blaabjerg, Frede; Franke, Toke; Tonnes, Michael; Lau, Mogens

*Published in:*  
I E E E Transactions on Power Electronics

*DOI (link to publication from Publisher):*  
[10.1109/TPEL.2014.2374652](https://doi.org/10.1109/TPEL.2014.2374652)

*Publication date:*  
2015

*Document Version*  
Accepted author manuscript, peer reviewed version

[Link to publication from Aalborg University](#)

*Citation for published version (APA):*  
Zhou, D., Blaabjerg, F., Franke, T., Tonnes, M., & Lau, M. (2015). Reduced Cost of Reactive Power in Doubly Fed Induction Generator Wind Turbine System With Optimized Grid Filter. *I E E E Transactions on Power Electronics*, 30(10), 5581-5590. <https://doi.org/10.1109/TPEL.2014.2374652>

### **General rights**

Copyright and moral rights for the publications made accessible in the public portal are retained by the authors and/or other copyright owners and it is a condition of accessing publications that users recognise and abide by the legal requirements associated with these rights.

- Users may download and print one copy of any publication from the public portal for the purpose of private study or research.
- You may not further distribute the material or use it for any profit-making activity or commercial gain
- You may freely distribute the URL identifying the publication in the public portal -

### **Take down policy**

If you believe that this document breaches copyright please contact us at [vbn@aub.aau.dk](mailto:vbn@aub.aau.dk) providing details, and we will remove access to the work immediately and investigate your claim.



# Reduced Cost of Reactive Power in Doubly Fed Induction Generator Wind Turbine System with Optimized Grid Filter

Dao Zhou, *Member, IEEE*, Frede Blaabjerg, *Fellow, IEEE*, Toke Franke, *Member, IEEE*, Michael Tonnes, and Mogens Lau

zda@et.aau.dk, fbl@et.aau.dk, toke.franke@danfoss.com, michael.tonnes@danfoss.com, mogens.lau@siemens.com

**Abstract**—The modern grid requirement has caused that the wind power system behaves more like conventional rotating generators and it is able to support certain amount of the reactive power. For a typical doubly-fed induction generator wind turbine system, the reactive power can be supported either through the rotor-side converter or the grid-side converter. This paper firstly compares the current ripples and supportive reactive power ranges between the conventional L and optimized LCL filter, if the reactive power is injected from the grid-side converter. Then, the loss distribution is evaluated both for the generator and the wind power converter in terms of the reactive power done by the rotor-side converter or the grid-side converter with various grid filters. Afterwards, the annual energy loss is also estimated based on yearly wind profile. Finally, experimental results of the loss distribution are performed in a down-scaled DFIG system. It is concluded that over-excited reactive power injected from the grid-side converter has lower energy loss per year compared to the over-excited reactive power covered by the rotor-side converter. Furthermore, it is also found that the annual energy loss could even become lower with the optimized filter and thereby more energy production for the wind turbine.

## I. INTRODUCTION

The voltage-source converter is widely used as an interface for the renewable energy systems before they are linked to the grid like in the photovoltaic and wind power system cases, with its advantages in fully control of dc-link voltage, active and reactive power as well as power factor [1]–[3]. A grid filter is normally introduced to avoid the PWM carrier and side-band voltage harmonics coupling to the grid that can disturb other sensitive loads or equipment. For the MW-level wind power converter, due to the quite low switching frequency of the power switching devices (usually several kilo-Hertz), a simple filter inductor consequently becomes bulky, expensive and it may also bring poorer dynamics into the system [4]–[6].

In order to fulfill the modern grid codes [7]–[9], the wind turbine system is currently required to behave more like a traditional power source (e.g. synchronous generator), which implies that the wind turbine system should have the capability of reactive power support. Due to the doubly-fed mechanism of the Doubly-Fed Induction Generator (DFIG)

based wind turbine system, the reactive power can be supported either by the Grid-Side Converter (GSC) or the Rotor-Side Converter (RSC). If the reactive power is provided by the GSC, in case of the constant dc-link voltage, the modulation index is closely related to the filter inductance, and it will increase very fast to over-modulation, especially when over-excited reactive power is needed [10]. There are two ways to deal with this issue – increase the dc-link voltage, which gives higher switching loss and power rating, or design an optimized grid filter.

Besides, if a small amount of reactive power is demanded by the transmission system operator, it is also of interest to compare the loss of the whole DFIG system, as the reactive power supported by the GSC only affects the loss of the GSC, while the reactive provided by the RSC not only influences the loss of the RSC, but also the loss of the generator itself. Then, the annual energy loss of the wind turbine system and cost of the reactive power can be calculated based on the annual wind profile at different compensation schemes.

The structure of the paper is organized as the following. Section II addresses the function of the grid filter in terms of the grid current ripple and the reactive power range. Then the LCL filter design procedure and the characteristic comparison between the L filter and the LCL filter are discussed in Section III. The loss model and loss distribution of the DFIG system in the case of over-excited reactive power injection is followed in Section IV. According to an annual wind profile, Section V discusses the energy loss per year. Finally, after the loss distribution of different parts in the DFIG system is measured on a 7.5 kW test rig in Section VI, some concluding remarks are drawn in Section VII.

## II. FUNCTIONS OF GRID FILTER

One of the most popular concepts in the mainstream wind power system market is the DFIG configuration as shown in Fig. 1. Except for the advantage that the back-to-back power converters take up only the slip power of the DFIG, this configuration has two possibilities to deliver the demanded reactive power, either from the generator's stator  $Q_s$  controlled by the RSC or from the GSC  $Q_g$  [10]. Since the

inductance difference for the secondary and tertiary winding of the three-winding transformer affects the amount of reactive power transmitted to the power grid, the three winding ratio is assumed as 1:1:1 for simplicity. The control of the back-to-back power converter is described in [11].

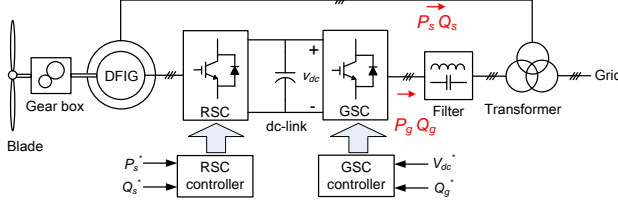


Fig. 1. Typical DFIG configuration in a wind turbine system (GSC: Grid-Side Converter, RSC: Rotor-Side Converter).

As recommended in IEEE 519-1992, harmonics higher than 35th should be explicitly limited [12]. If a simple L filter is assumed to be used, the current ripple amplitude is jointly decided by the dc-link voltage, the switching frequency and inductance value [13]. For a typical 2 MW DFIG based wind turbine system, the main parameters of which are listed in TABLE I, the relationship between the current ripple and the active power of GSC  $P_g$  is shown in Fig. 2(a). It is noted that as expected the higher inductance is, the lower switching current ripple will be.

TABLE I  
BASIC PARAMETERS OF A 2 MW DFIG SYSTEM

Rated power $P_s$	2 MW
Range of DFIG rotor speed $n_r$	1050 – 1800 rpm
Line frequency $f_l$	50 Hz
Rated line voltage amplitude $U_{gm}$	563 V
DC-link voltage $U_{dc}$	1050 V
Switching frequency $f_s$	2 kHz

As aforementioned, if the reactive power is required from the grid, the value of the filter inductance also affects the modulation index. Fig. 2(b) indicates the relationship between the dc-link voltage and the reactive power of the GSC  $Q_g$  (the fully modulation index is assumed). In order to fulfill the reactive power range stated in E.ON Netz [7], the DFIG system should cover up to 0.4 pu Over-Excited (OE) and 0.3 pu Under-Excited (UE) reactive power in respect to the generator power rating. As the pu value is normally defined by the power rating of the induction generator, the used pu value in Fig. 2(b) becomes 2.0 pu OE and 1.5 pu UE reactive power in respect to the GSC, which is five times higher than the pu value seen from the induction generator due to the rated slip power through the GSC. It can be seen that the minimum dc-link voltage increases considerably with higher inductance if the OE reactive power is needed. On the other hand, the higher inductance results in a lower switching ripple. Thus, it is a trade-off procedure of the grid filter design. For the DFIG system as shown in Fig. 1, since

the final current ripple to the power grid is calculated as the sum of the stator current and the GSC current, and the stator current is much higher than the GSC current, 40% current ripple at the GSC is acceptable and it is used as the design criteria, which implies the filter inductance is selected at 0.1 pu.

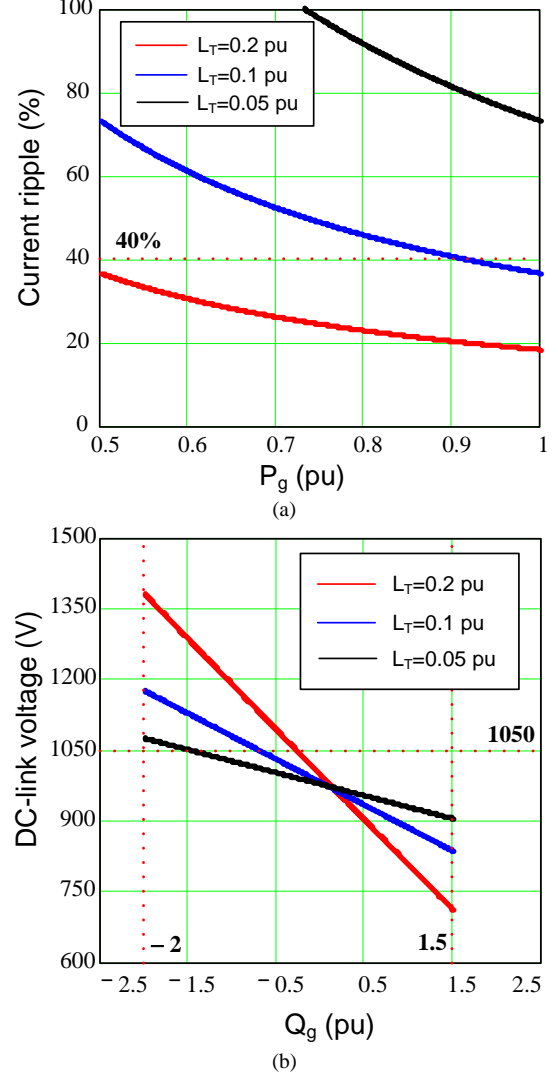


Fig. 2. Influence of grid filter inductance on the GSC performance. (a) Current ripple rate; (b) Reactive power range.

### III. CHARACTERISTIC COMPARISON OF AN L AND LCL FILTER

The equivalent single-phase GSC with an LCL filter is shown in Fig. 3, which typically has no additional sensors compared to the conventional L filter configuration. Although the different positions of the voltage and current sensors may have their own advantages [13], the current sensors on the converter side is chosen, because it can be designed to protect the power semiconductor and it is commonly used in industrial application.

### A. Design procedure of LCL filter

As shown in Fig. 3,  $L_c$  is the converter side inductance,  $L_f$  is the grid side inductance, and  $C_f$  is the capacitor bank, which is connected to a damping resistance  $R_d$ . The converter current and the grid current are represented by  $i$  and  $i_g$ . Moreover, the voltage of the converter output and the point of common coupling are represented by  $v_i$ ,  $v_g$ , respectively.

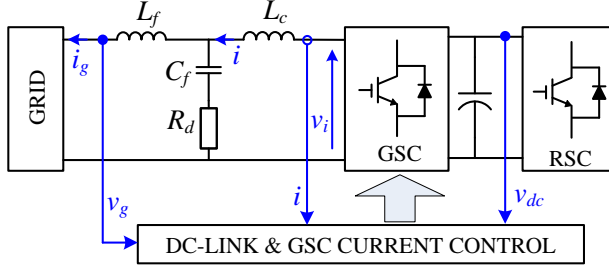


Fig. 3. Equivalent single-phase grid-side converter with LCL filter.

A step-by-step design procedure for LCL filter is described in [3]. This design is focused on that the total inductance of the LCL filter is able to reduce to half compared to the L filter. Afterwards, a proper inductance sharing into  $L_c$  (0.025 pu) and  $L_g$  (0.025 pu) is realized in order to achieve the desired current ripple reduction. The capacitance value (0.1 pu) is then determined by the absorbed reactive power at the rated conditions, in which the resonant frequency becomes 1.35 kHz (67.5% of  $f_{sw}$ ). The passive damping is inevitably designed to overcome the resonant problem, where its power dissipation is also taken into account [3], [13]-[15]. The used filter parameters are summarized in TABLE II.

TABLE II  
L AND LCL FILTER PARAMETERS

L filter	Filter inductor $L_f$	500 $\mu$ H
LCL filter	Converter-side inductor $L_c$	125 $\mu$ H
	Grid-side inductor $L_f$	125 $\mu$ H
	Filter capacitor $C_f$	220 $\mu$ F
	Damping $R_d$	0.5 m $\Omega$

### B. Characteristic comparison between L and LCL filter

If the transfer function of the PI current controller, the modulation unit as well as some delays introduced by the digital control are considered, the open-loop Bode plots of the L and the LCL filter from the GSC current reference to the line current is then shown in Fig. 4. It is clear that the magnitude and phase characteristic between the L and LCL filter are exactly the same at lower frequency, if the PI parameter used in the current controller is under proper design. It is also noted that the smaller magnitude of the LCL filter appears at the switching frequency compared to the L filter. Moreover, the damping of the LCL filter has a better

performance compared to the L filter above the switching frequency as expected.

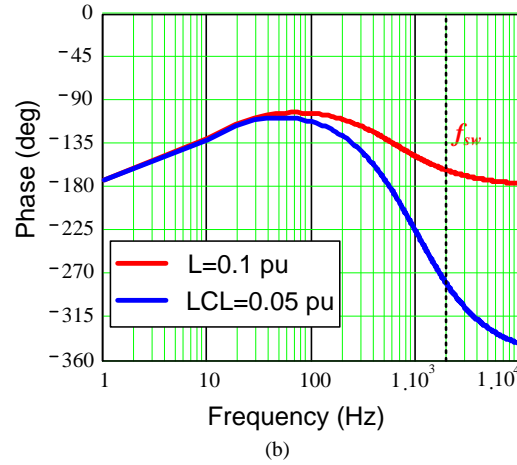
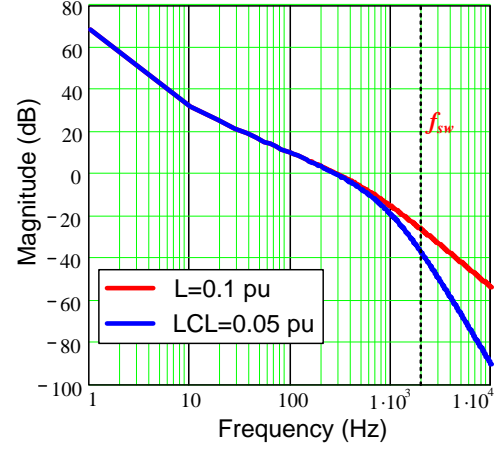


Fig. 4. Bode plot comparison between pure L filter (0.1 pu) and designed LCL filter (0.05 pu). (a) Magnitude diagram; (b) Phase diagram.

## IV. LOSS BREAKDOWN OF DFIG SYSTEM

The reactive power injection basically consists of the OE reactive power and the UE reactive power. As analyzed in [16], the specific OE reactive power injection decreases the efficiency of the DFIG system. Consequently, only this kind of reactive power operation is in focus in this paper.

### A. Loss model of DFIG system

As shown in Fig. 1, the common-adopted methodology to compensate the reactive power is from the stator of the induction generator, due to the fact that it introduces a small increase of the rotor-side current because of the winding ratio between the stator and the rotor of the DFIG [17]. However, this approach not only affects the loss of the RSC, but also imposes the loss of the DFIG itself.

Loss dissipation inside the induction generator generally consists of the copper loss and iron loss as shown in Fig. 5 [18]. If the stator voltage oriented vector control is applied, the stator-side active power  $P_s$  and reactive power  $Q_s$  are

independently in line with the stator d-axis current  $i_{sd}$  and q-axis current  $i_{sq}$ . Due to the flux equation existing in the DFIG, the relationship between the rotor and stator current under d-axis and q-axis are,

$$\begin{cases} \dot{i}_{rd} = -\frac{L_{ls} + L_m}{L_m} \dot{i}_{sd} \\ \dot{i}_{rq} = -\frac{U_{gm}}{\omega_1 \cdot L_m} - \frac{L_{ls} + L_m}{L_m} \dot{i}_{sq} \end{cases} \quad (1)$$

where  $L_{ls}$  and  $L_m$  denote the stator leakage inductance and the magnetizing inductance,  $U_{gm}$  denotes the rated grid phase-voltage,  $\omega_1$  is the fundamental electrical angular frequency, and the subscript  $d$  and  $q$  denote the value at d-axis and q-axis circuit, respectively.

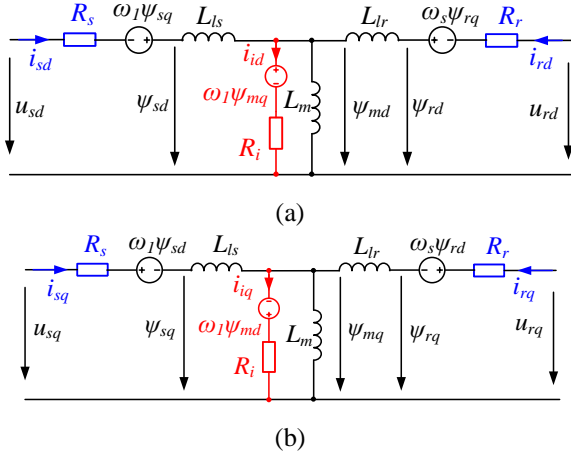


Fig. 5. DFIG equivalent circuit considering copper loss and iron loss. (a) d-axis circuit; (b) q-axis circuit.

The copper loss  $P_{cu}$  is resistive losses occurring in the winding coils and can be calculated using the equivalent d-q axis circuit stator resistance  $R_s$  and rotor resistance  $R_r$  as shown in Fig. 5,

$$P_{cu} = \frac{3}{2} \cdot [(i_{sd}^2 + i_{sq}^2) \cdot R_s + (i_{rd}^2 + i_{rq}^2) \cdot R_r] \quad (2)$$

where  $i_s$  and  $i_r$  denote the stator current and the rotor current. It can be seen that the copper loss of the induction generator is jointly dependent on the stator active power and reactive power.

Generally, the iron loss is produced by the flux change, and it consists of eddy current loss and hysteresis loss, both of which are tightly connected with the operation frequency and flux density [18]. This method needs to know the empirical formula in advance, and the calculation is normally done according to the Finite Element Method (FEM). Alternatively, iron losses can be estimated from the electrical point of view [8], [20]. In other words, it can be expressed by the equivalent iron resistance  $R_i$  in parallel with the magnetizing inductance as shown in Fig. 5.

The voltage equations for the additional iron resistor are,

$$\begin{cases} R_i \cdot i_{id} = \frac{d\psi_{md}}{dt} - \omega_1 \cdot \psi_{mq} \\ R_i \cdot i_{iq} = \frac{d\psi_{mq}}{dt} + \omega_1 \cdot \psi_{md} \end{cases} \quad (3)$$

where  $i_i$  is the equivalent iron loss current,  $\psi_m$  is the magnetizing flux. Moreover, with the aid of the relationship between the stator flux and magnetizing flux,

$$\begin{cases} \psi_{md} = \psi_{sd} - L_{ls} \cdot i_{sd} \\ \psi_{mq} = \psi_{sq} - L_{ls} \cdot i_{sq} \end{cases} \quad (4)$$

where  $\psi_s$  denotes the stator flux.

Due to the stator voltage orientation,  $\psi_{md}$  is nearly zero, and  $\psi_{mq}$  is a constant value because of the stiff grid with the constant voltage and constant frequency. Substituting (4) into (3), the iron current can be deduced,

$$\begin{cases} i_{id} = \frac{\omega_1 L_{ls}}{R_i} \cdot i_{sq} + \frac{U_{gm}}{R_i} \\ i_{iq} = -\frac{\omega_1 L_{ls}}{R_i} \cdot i_{sd} \end{cases} \quad (5)$$

According to (5), it is noted that the d-axis iron loss current depends on the reactive power  $Q_s$ , while the q-axis iron loss current is related with the active power  $P_s$ . As a consequence, the iron loss  $P_{fe}$  can be calculated as,

$$P_{fe} = \frac{3}{2} \cdot [(i_{id}^2 + i_{iq}^2) \cdot R_i] \quad (6)$$

In respect to the losses of the power converters in the DFIG system, it is well described in [16]. If the reactive power is provided by the RSC, the loss model of the generator (copper loss and iron loss) and the RSC (conduction loss and switching loss both in the IGBT and the freewheeling diode) is shown in Fig. 6(a). It is evident that if the references of the active power, reactive power and slip are known in advance, together with the information of the generator and power switching devices, each type of the losses can be analytically calculated.

With the aid from the GSC, another approach may be realized to compensate the reactive power, which stresses the GSC and affects the loss of the GSC and the filter. Compared with the GSC losses, the grid filter loss is small enough [21], and it is simply calculated by its parasitic Equivalent Series Resistance (ESR). Similarly, as the conduction loss and switching loss of the IGBT and the diode are analytically solved, thus the GSC loss can be calculated as shown in Fig. 6(b).

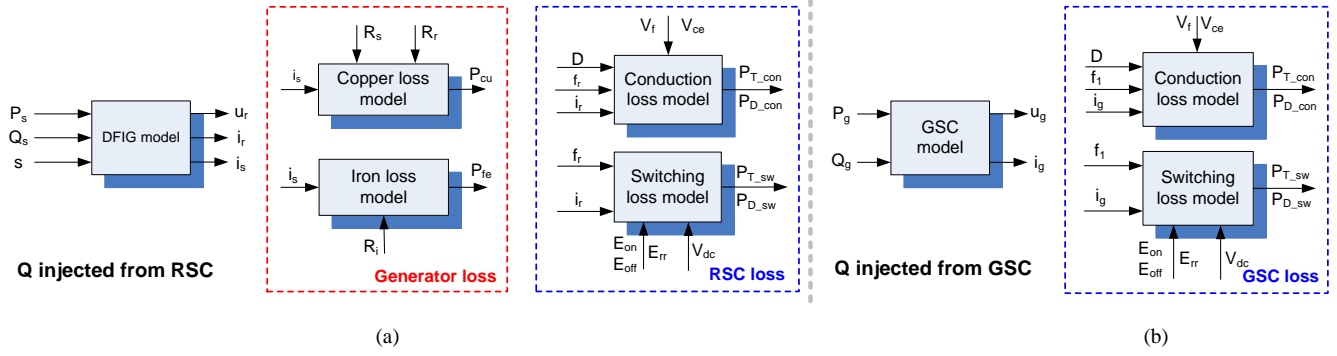


Fig. 6. Framework of power loss estimation. (a) Reactive power is injected by the RSC; (b) Reactive power is injected by the GSC.

### B. Loss breakdown of DFIG system

The loss distribution of the whole DFIG system is firstly evaluated at the normal operation (NOR), i.e. no reactive power is exchanged between the DFIG system and the grid. Then, the loss distribution is given in cases that the OE reactive power is fully from the RSC (OE\_RSC) or the GSC. As the type of the grid filter only influences the loading of the GSC, it can be further divided by L filter (OE\_L\_GSC) and LCL filter (OE\_LCL\_GSC). The above cases are summarized in TABLE III. It is worth to mention that the dc-link voltage can be different at various compensation schemes which is consistent with Fig. 2(b). It can be seen that the OE\_L\_GSC has a higher dc voltage than the OE\_LCL\_GSC, due to the higher total inductance of the filter.

TABLE III

CASES FOR NORMAL OPERATION AND OVER-EXCITED REACTIVE POWER INJECTION

	$Q_s$ (pu)	$Q_g$ (pu)	$U_{dc}$ (V)
NOR	0	0	1050
OE_RSC	0.4	0	1050
OE_L_GSC	0	0.4	1250
OE_LCL_GSC	0	0.4	1100

The loss breakdown at the rated power of the four cases in terms of the DFIG, the RSC, the GSC and its filter is then shown in Fig. 7. In respect to the generator loss, together with the parameters of the DFIG listed in TABLE IV, it can be seen that the generator losses (especially copper losses) increase only in the OE\_RSC compared to the NOR in Fig. 7(a), because the reactive power injection by the RSC changes the generator's stator and rotor current amplitude. In respect to the RSC losses, it also increases considerably in the OE\_RSC. Moreover, the power loss (especially the switching loss) increases slightly in OE\_L\_GSC and OE\_LCL\_GSC compared to NOR operation, since the dc-link voltage becomes higher. For the GSC losses, OE\_RSC stays the same with the NOR operation. However, if the reactive power is supported by the GSC, both the conduction losses and the switching losses increase significantly because of the dominating reactive current, and it also becomes three

times higher than in the case that the reactive power is injected by the RSC. The tendency of the grid filter loss is similar to the GSC because of the same current through them. It is noted that if the OE reactive power is compensated from the GSC, the LCL filter consumes lower power loss due to the smaller ESR compared to the pure L filter. For the loss distribution of the whole DFIG system, compared with the loss of the DFIG itself and the power converters, the loss dissipated in the DFIG is dominant.

From another perspective - if no reactive power is required, the power loss of various parts in the DFIG system at different wind speeds are shown in Fig. 8 (assuming that after 11 m/s wind turbine is operating at full load). In Fig. 8(a), it is noted that the iron loss stays almost constant at various wind speeds, while the copper loss changes dynamically. For the RSC losses shown in Fig. 8(b), it increases with the higher wind speed. In respect to the GSC losses at different wind speeds, it can be seen that the power loss becomes low at 8 m/s, which is regarded as the synchronous operation as shown in Fig. 8(c). The loss of the grid filter is much smaller than the GSC as shown in Fig. 8(d). Besides, the loss distribution of the whole DFIG system is shown in Fig. 8(e).

TABLE IV

2 MW GENERATOR AND BACK-TO-BACK POWER CONVERTER

Generator	Rated power $P_s$	2 MW
	Rated line voltage $U_{sm}$	563 V
	Stator leakage inductance $L_{ls}$	0.050 pu
	Rotor leakage inductance $L_{lr}$	0.085 pu
	Magnetizing inductance $L_m$	3.840 pu
	Stator resistance $R_s$	0.007 pu
	Rotor resistance $R_r$	0.006 pu
	Equivalent iron loss resistance $R_i$	99.853 pu
	Ration of stator and rotor winding	0.369
Power converters	Used power module	1 kA/1.7 kV
	Grid-side converter	Single
	Rotor-side converter	Two in parallel

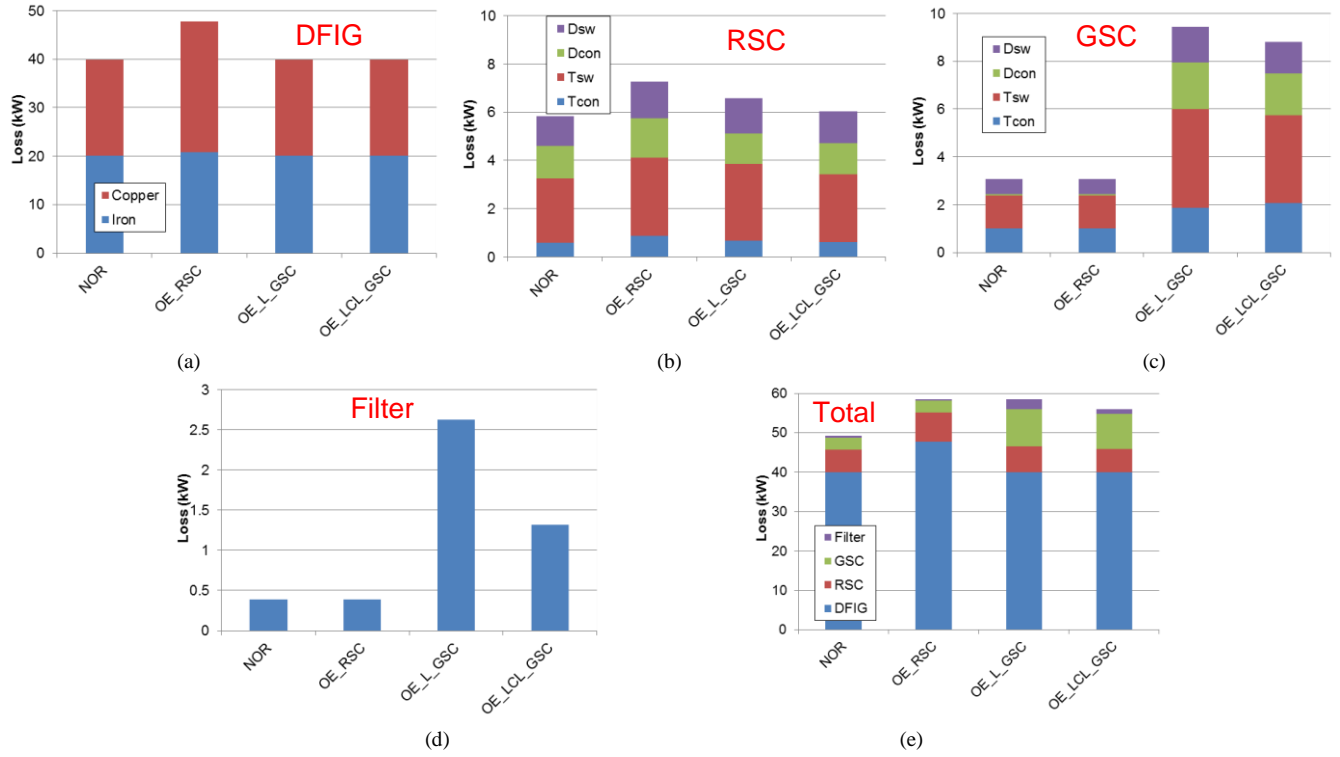


Fig. 7. Loss breakdown at rated wind speed (11 m/s) with various reactive power compensation schemes. (a) DFIG itself; (b) Rotor-side converter; (c) Grid-side converter; (d) Grid filter; (e) Total system.

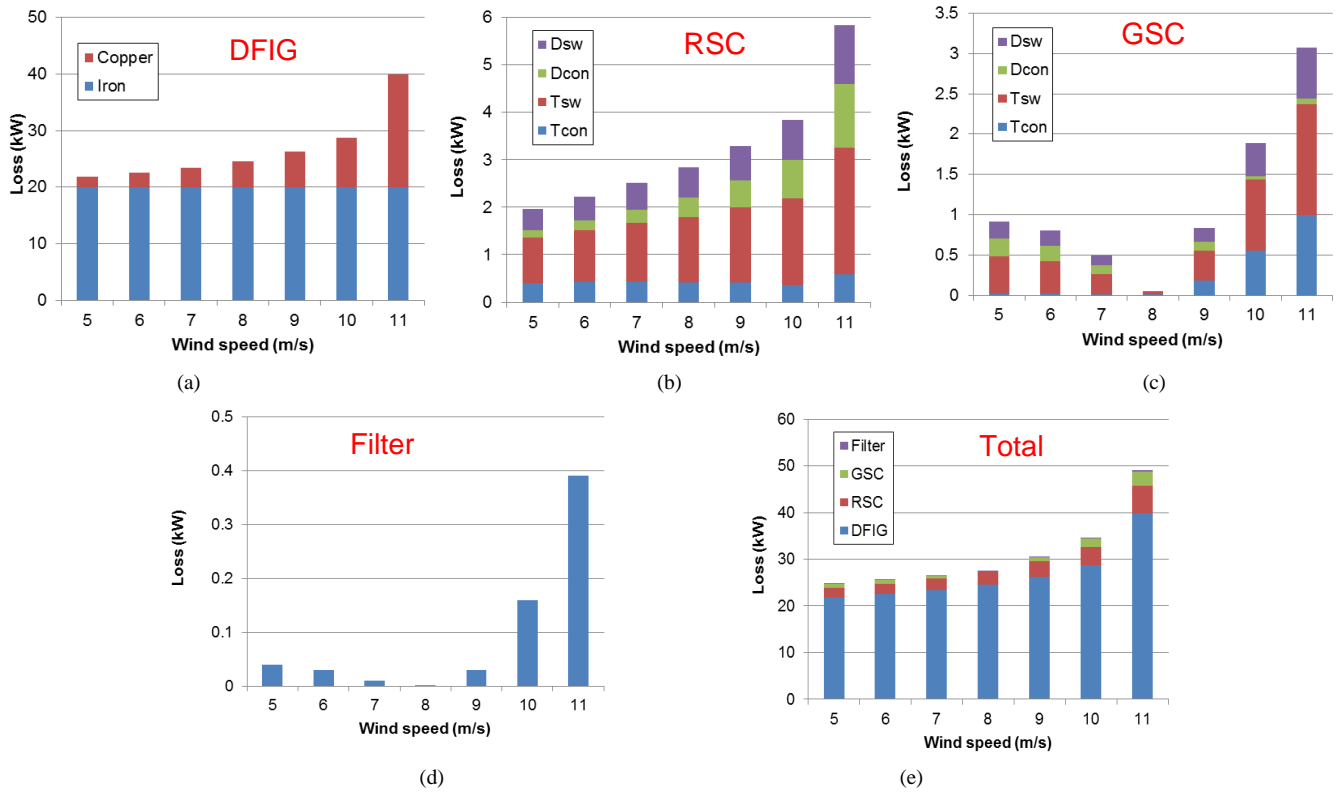


Fig. 8. Loss breakdown at normal operation (NOR) with different wind speeds. (a) DFIG itself; (b) Rotor-side converter; (c) Grid-side converter; (d) Grid filter; (e) Total system.



## V. ENERGY LOSS BASED ON ANNUAL WIND PROFILE

Based on the power loss model and the loss distribution with various amounts of reactive power described in Section IV, this section further estimates the energy loss and cost of reactive power according to an annual wind profile.

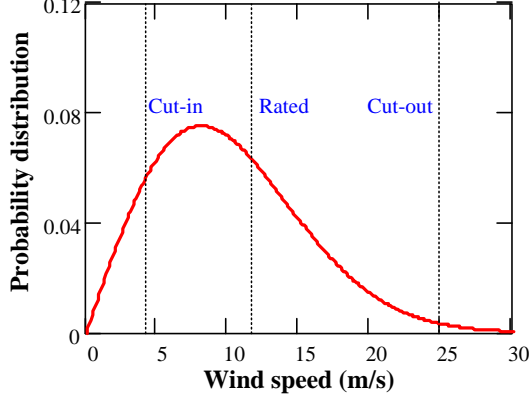


Fig. 9. Class I annual wind distribution defined by IEC standard [22].

The annual wind of Weibull distribution according to the IEC standard - Class I [22], [23] with the mean wind speed 10 m/s is shown in Fig. 9. As each loss (kW) at various wind speeds can be calculated by a wind speed step of 1 m/s as shown in Fig. 8, as well as the yearly wind speed distribution (hours), the annual loss of energy can be calculated. It is worth to mention that the annual loss of energy is only concerned from the cut-in to the rated wind speed, because if the wind speed is higher than rated value, it is assumed that the power loss dissipated (loss of energy production) in the DFIG system can be compensated by the mechanical power from the wind turbine blades.

The annual energy loss of the DFIG system at various operation modes is shown in Fig. 10(a). It is evident that the energy consumed by the induction generator is much higher than in the back-to-back power converters. Moreover, it can be seen that, although the OE reactive power compensation from the GSC significantly imposes the loading of the GSC itself and its filter, the OE\_LCL\_GSC still has the lowest loss of energy.

It is also an interesting perspective to express the annual energy loss in terms of the percentage over the yearly produced energy, which is accumulated from the cut-in until the cut-off wind speed. As shown in Fig. 10(b), under the assumption that the OE reactive power is required all year around, the normal case is the OE\_RSC that takes up 2.05% annual energy, while the best situation is achieved by the OE\_LCL\_GSC 1.98%, which implies 3.41% energy saving per year.

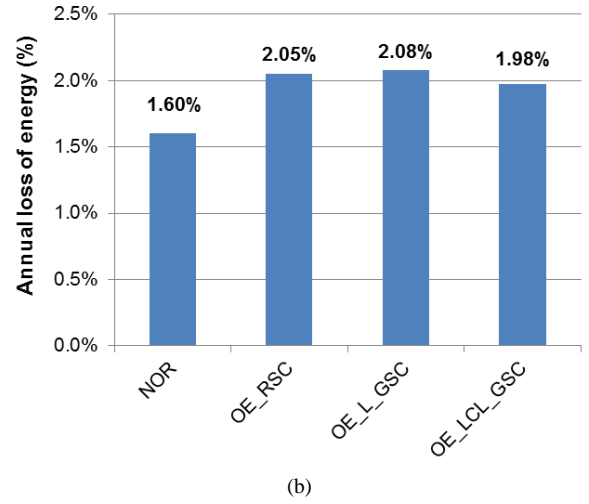
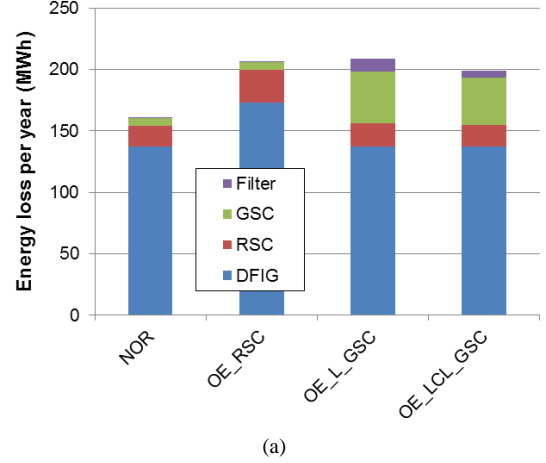


Fig. 10. Annual loss of energy in normal operation and if the OE reactive power is required all year around. (a) Energy loss per year (MWh); (b) Annual loss of energy (%).

## VI. EXPERIMENTAL VERIFICATION OF LOSS DISSIPATION

In order to validate the loss dissipation of the DFIG system at different reactive power compensation methods, a down-scaled 7.5 kW test rig is built up and shown in Fig. 11. The DFIG is externally driven by a prime motor, and two 5.5 kW Danfoss motor drives are used for the GSC and the RSC, both of which are controlled with dSPACE 1006. Besides, the LCL filter is employed as the grid filter, whose capacitor branch can be bypassed to realize the L type filter. The important parameters of the test setup are summarized in TABLE V. It is noted that, as the rated rotor speed is 1800 rpm, the pu value of the grid filter is calculated based on the slip power of the DFIG.

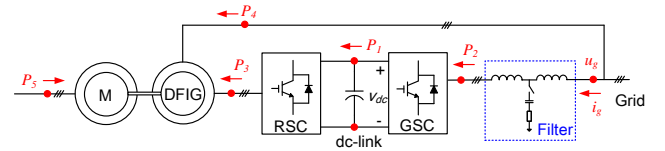


Fig. 11. Setup of 7.5 kW DFIG test rig.

TABLE V  
7.5 kW GENERATOR AND 5.5 kW BACK-TO-BACK POWER CONVERTER

Generator	Rated power	7.5 kW
	Rated line voltage	380 V
	Stator leakage inductance	0.056 pu
	Rotor leakage inductance	0.084 pu
	Magnetizing inductance	1.294 pu
	Stator resistance	0.022 pu
	Rotor resistance	0.033 pu
	Equivalent iron loss resistance	35.734 pu
	Ratio of stator and rotor winding	0.336
Power converters	Rated power	5.5 kW
	Grid-side converter rated current	10 A
	Rotor-side converter rated current	10 A
	Switching frequency	5 kHz
Grid filters	L type	
	Interface inductance $L_l$	5.9% pu
	LCL type	
	Converter-side inductor $L_c$	3.6% pu
	Grid-side inductor $L_f$	2.3% pu
	Filter capacitor $C_f$	20.0% pu
	Damping $R_d$	13.4% pu

In the condition that the full power of the DFIG is realized at 1800 rpm, 0.4 pu reactive power according to the grid codes is compensated from the GSC, the current injecting to the grid from the back-to-back power converter is compared with the LCL and L filter as shown in Fig. 12. It is noted that the fundamental currents of the L and the LCL filter both are 4.2 A, and the currents are leading the grid voltage 90 degree, as the majority of which belongs to the reactive component. Furthermore, the maximum value of the harmonic spectrum around the switching frequency is 105 mA with the L filter, which is much higher than the LCL filter 25 mA.

The loss dissipation of the various parts in the down-scaled DFIG system is monitored by Yokogawa Power Analyzer WT3000. The loss of the DFIG itself, the RSC, the GSC and the grid filter are tested separately and they are shown in Fig. 13, in which four conditions are taken into account consistent with Fig. 7. It is worth to mention that the dc-link used in the above four cases is 600 V, 600 V, 750 V and 650 V, respectively. In respect to the loss of the DFIG itself and the RSC, it consumes the highest in the case that the reactive power is compensated from the RSC. However, regarding the GSC, the reactive power supported by the GSC with the L filter leads to the highest power loss, and similar filter loss can be observed in the cases of the reactive power compensation by the GSC because of the same value between the L and LCL filter.

The experimental result of total loss dissipation in the DFIG system at 1800 rpm is then shown in Fig. 14. Compared with Fig. 7(e), since the loss consumed in the DFIG actually contains both the DFIG loss and prime motor loss, the loss distribution of the DFIG is much higher compared to power converters. Moreover, it can be seen that the both OE\_L\_GSC and OE\_LCL\_GSC are more efficient than OE\_RSC due to the different amounts of the equivalent loss resistors between the 2 MW and 7.5 kW DFIGs.

## VII. CONCLUSION

This paper has studied the influence of the grid filter inductance on the current ripple and the reactive power range for a DFIG wind turbine system. Then, an optimized LCL filter design is achieved with half value of the total inductance compared to the pure L filter.

Due to the existence of the two possibilities to generate the demanded reactive power for the DFIG system – controlled by the rotor-side converter or controlled by the grid-side converter, each of them is analyzed in terms of the DFIG loss and the power converters loss. It is concluded that although the compensation from the grid-side converter significantly increases the power loss of the grid-side converter itself, it will still have lower total loss dissipation of the whole DFIG system, as the compensation approach by the rotor-side converter will impose the DFIG loss as well as the rotor-side converter loss.

Based on a typical annual wind speed distribution, the loss of energy per year is finally discussed. It can be seen that the injection of reactive power is actually not free-of-charge. Assuming the cost the offshore wind power is 0.2 Euro/kWh, compared with the normal operation of 1.60% annual energy loss (32.2k Euro), if the over-excited reactive power is injected by the rotor-side converter, it will increase to 2.05% annual energy loss (41.3k Euro) when the reactive power is needed all year around. On the other hand, if the grid filter is properly designed and the over-excited reactive power is supported by the grid-side converter, the annual energy loss becomes 1.98% (39.7k Euro), which implies 3.41% (1.6k Euro) energy saving per year compared to the over-excited reactive injected by the rotor-side converter.

## REFERENCES

- [1] A. A. Rockhill, M. Liserre, R. Teodorescu, P. Rodriguez, "Grid-filter design for a multi-megawatt medium-voltage voltage-source inverter," *IEEE Trans. Industrial Electronics*, vol. 58, no. 4, pp. 1205-1217, Apr. 2011.
- [2] M. Liserre, F. Blaabjerg, A. Dell'Aquila, "Step-by-step design procedure for a grid-connected three-phase PWM voltage source converter," *International Journal of Electronics*, 91(8), pp. 445-460, Jan. 2004.
- [3] M. Liserre, F. Blaabjerg, S. Hansen, "Design and control of an LCL-filter-based three-phase active rectifier," *IEEE Trans. Industry Applications*, vol. 41, no. 5, pp. 1281-1291, Sep. 2005.
- [4] Z. Chen, J. M. Guerrero, F. Blaabjerg, "A review of the state of the art of power electronics for wind turbines," *IEEE Trans. Power Electronics*, vol. 24, no. 8, pp. 1859-1875, Aug. 2009.

- [5] F. Blaabjerg, Z. Chen, S. B. Kjaer, "Power electronics as efficient interface in dispersed power generation systems," *IEEE Trans. Power Electronics*, vol. 19, no. 5, pp. 1184-1194, Sep. 2004.
- [6] M. Liserre, R. Cardenas, M. Molinas, J. Rodriguez, "Overview of multi-MW wind turbines and wind parks," *IEEE Trans. Industrial Electronics*, vol. 58, no. 4, pp. 1081-1095, Apr. 2011.
- [7] E.ON-Netz. Requirements for offshore grid connections, Apr. 2008.
- [8] M. Tsili, S. Papathanassiou, "A review of grid code technical requirements for wind farms," *IET on Renewable Power Generation*, vol. 3, no. 3, pp. 308-332, Sep. 2009.
- [9] A. Camacho, M. Castilla, J. Miret, R. Guzman, A. Borrell, "Reactive power control for distributed generation power plants to comply with voltage limits during grid faults," *IEEE Trans. Power Electronics*, vol. 29, no. 11, pp. 6224-6234, Nov. 2014.
- [10] D. Zhou, F. Blaabjerg, M. Lau, M. Tonnes, "Thermal behavior optimization in multi-MW wind power converter by reactive power circulation," *IEEE Trans. Industry Applications*, vol. 50, no. 1, pp. 433-440, Jan. 2014.
- [11] S. Muller, M. Deicke, R. W. De Doncker, "Doubly fed induction generator systems for wind turbines," *IEEE Industry Applications Magazine*, vol. 8, no. 3, pp. 26-33, May 2002.
- [12] A. Nagel, R. W. De Doncker, "Systematic design of EMI-filters for power converters," in *Proc. of IAS 2000*, pp. 2523-2525, 2000.
- [13] R. Teodorescu, M. Liserre, P. Rodriguez, *Grid Converters for Photovoltaic and Wind Power Systems*. Hoboken, NJ, USA: Wiley, 2011.
- [14] R. Pena-Alzola, M. Liserre, F. Blaabjerg, R. Sebastian, J. Dannehl, F. W. Fuchs, "Analysis of the passive damping losses in LCL-filter-based grid converters," *IEEE Trans. Power Electronics*, vol. 28, no. 6, pp. 2642-2646, Jun. 2013.
- [15] W. Wu, Y. He, T. Tang, F. Blaabjerg, "A new design method for the passive damped LCL and LLCL Filter-based single-phase grid-tied inverter," *IEEE Trans. Industrial Electronics*, vol. 60, no. 10, pp. 4339-4350, Oct. 2013.
- [16] D. Zhou, F. Blaabjerg, M. Lau, M. Tonnes, "Thermal cycling overview of multi-megawatt two-level wind power converter at full grid code operation," *IEEE Journal of Industry Applications*, vol. 2, no. 4, pp. 173-182, Jul. 2013.
- [17] S. Engelhardt, I. Erlich, C. Feltes, J. Kretschmann, F. Shewarega, "Reactive power capability of wind turbines based on doubly fed induction generators," *IEEE Trans. Energy Conversion*, vol. 26, no. 1, pp. 364-372, Mar. 2011.
- [18] R. Takahashi, H. Ichita, J. Tamura, M. Kimura, M. Ichinose, M. Futami, K. Ide, "Efficiency calculation of wind turbine generation system with doubly-fed induction generator," in *Proc. of International Conference on Electrical Machines (ICEM) 2010*, pp. 1-4, 2010.
- [19] S. Wee, M. Shin, D. Hyun, "Stator-flux-oriented control of induction motor considering iron loss," *IEEE Trans. Industrial Electronics*, vol. 48, no. 3, pp. 602-608, Jun. 2001.
- [20] A. G. Abo-Khalil, H. Park, D. Lee, "Loss minimization control for doubly-fed induction generators in variable speed wind turbines," in *Proc. of IECON 2007*, pp. 1109-1114, 2007.
- [21] C. Sintamarean, F. Blaabjerg, H. Wang, "Comprehensive evaluation on efficiency and thermal loading of associated Si and SiC based PV inverter applications," in *Proc. of IECON 2013*, pp. 555-560, 2013.
- [22] Wind turbines – part I: design requirements", IEC 61400-1, 3rd edition.
- [23] Vestas website (Available at: <http://www.vestas.com/en/wind-power-plants/wind-project-planning/siting/wind-classes.aspx?action=3#/vestas-univers>).

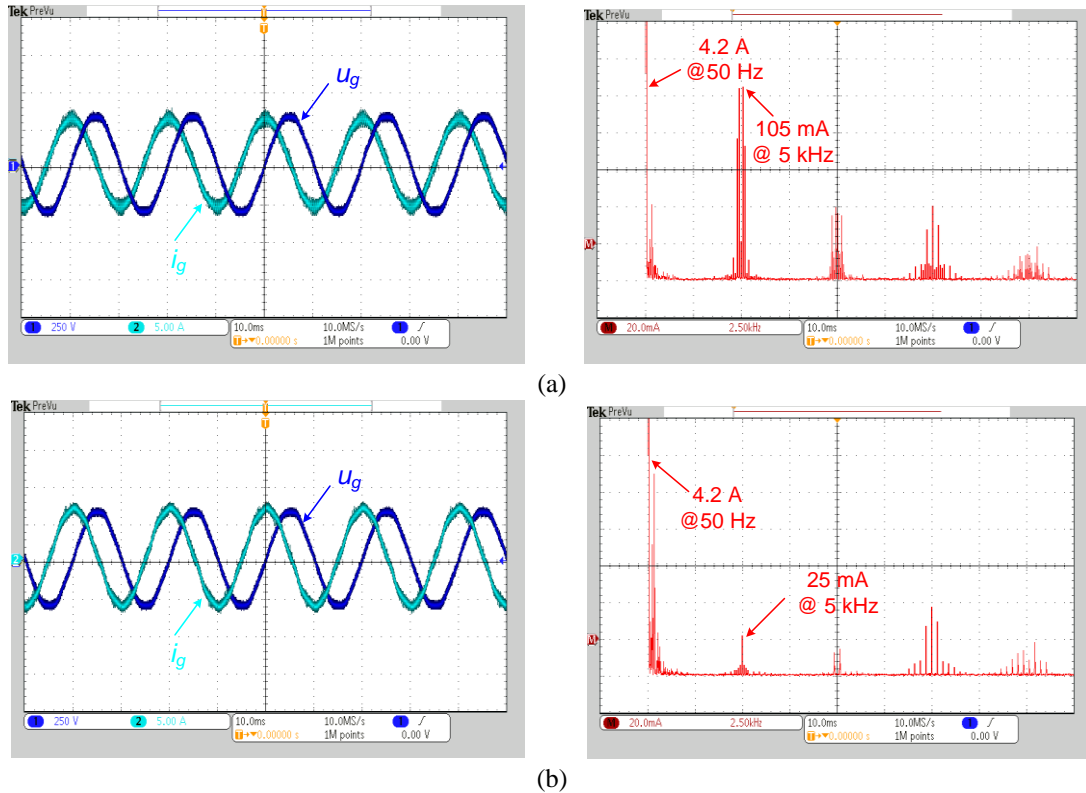


Fig. 12. Waveform and the harmonic of the grid current. (a) L filter; (b) LCL filter.

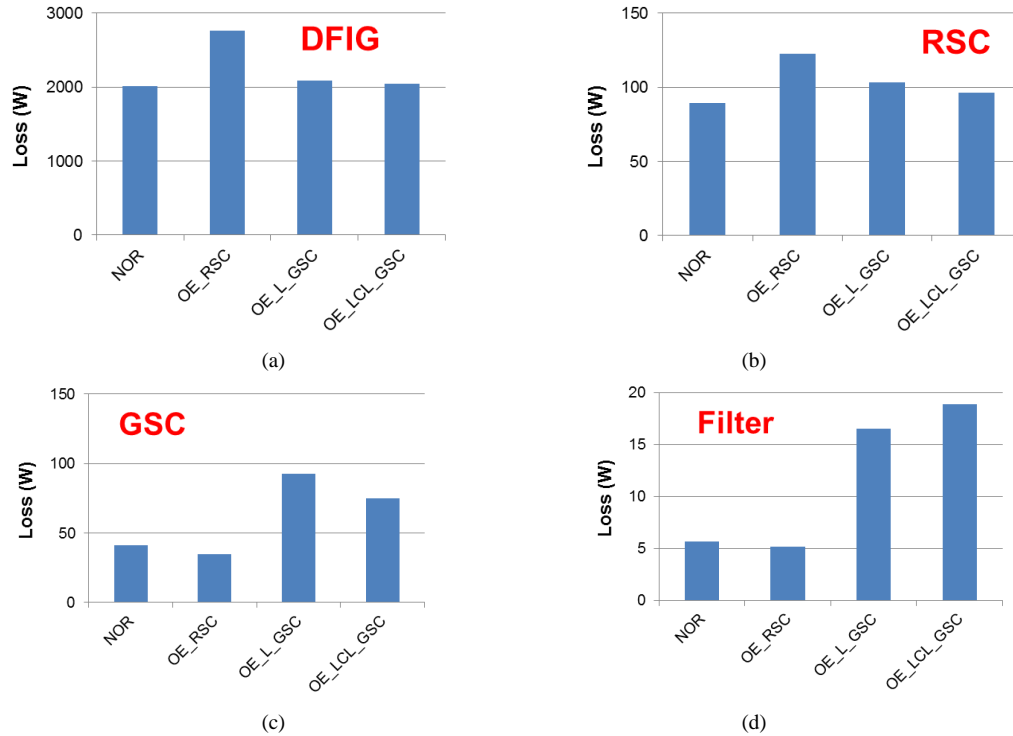


Fig. 13. Measured loss dissipation in the DFIG system at 1800 rpm in case of the normal operation and the various reactive power compensation schemes. (a) DFIG itself; (b) Rotor-side converter; (c) Grid-side converter; (d) Grid filter.

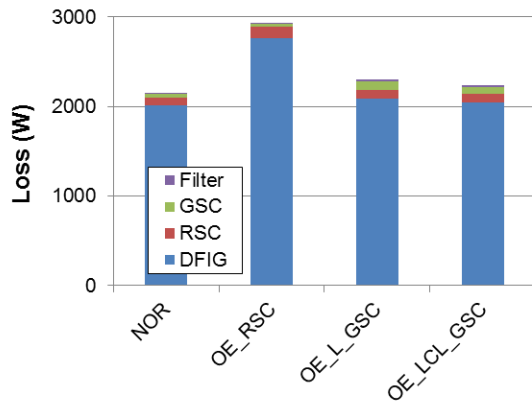
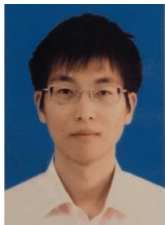


Fig. 14. Experimental result of total loss dissipation in the DFIG system at 1800 rpm in case of the normal operation and the various reactive power compensation schemes.



**Dao Zhou** (S'12) received the B.Sc. in electrical engineering from Beijing Jiaotong University, Beijing, China, in 2007, and the M. Sc. in power electronics from Zhejiang University, Hangzhou, China, in 2010. From 2012, he is pursuing the Ph.D degree in the Department of Energy Technology, Aalborg University, Aalborg, Denmark.

His research interests include two-level power electronics converters and their application in wind power generation systems.



**Frede Blaabjerg** (S'86-M'88-SM'97-F'03) was with ABB-Scandia, Randers, Denmark, from 1987 to 1988. From 1988 to 1992, he was a PhD student with Aalborg University, Aalborg, Denmark. He became an Assistant Professor in 1992, an Associate Professor in 1996, and a Full Professor of power electronics and drives in 1998. His current research interests include power electronics and its applications such as in wind turbines, PV systems, reliability, harmonics and adjustable speed drives.

He has received 15 IEEE Prize Paper Awards, the IEEE PELS Distinguished Service Award in 2009, the EPE-PEMC Council Award in 2010, the IEEE William E. Newell Power Electronics Award 2014 and the Villum Kann Rasmussen Research Award 2014. He was an Editor-in-Chief of the IEEE TRANSACTIONS ON POWER ELECTRONICS from 2006 to 2012. He has been Distinguished Lecturer for the IEEE Power Electronics Society from 2005 to 2007 and for the IEEE Industry Applications Society from 2010 to 2011.



**Toke Franke** received the Dipl.-Ing. and Ph.D. degrees from Christian-Albrechts-University, Kiel, Germany in 2007 and 2013, respectively.

Between 2007 and 2011 he carried out research work at Christian-Albrechts-University on silicon carbide power devices in solar applications.

From 2011 to 2013 he was senior hardware technology engineer at Danfoss Solar Inverters there he focused on storage technologies and silicon

carbide power devices. In 2014 he joined Danfoss Silicon Power as senior engineer for power stacks. His main research interest includes power devices and high density power stacks for renewable energies.

Dr. Franke is member of the IEEE Power Electronics Society.



**Michael Tonnes** received the M.Sc. EE degree from Aalborg University, Denmark in 1987, and the Ph.D. degree from the Institute of Energy Technology in 1990.

He was employed by Danfoss in 1987 to perform the Ph.D work within auto-tuning and automatic control of non-linear electrical machines and worked within the technology area of Motor Controls.

Michael worked in US in Danfoss High Power Drives for the period 1996-98 and had various management positions within electronic businesses. At present he is Senior Director of R&D at Danfoss Silicon Power GmbH with base in Flensburg, Germany.

He is author and co-author on a number of articles within auto-tuning, motor controls and power electronics in general and holds several patents within the field motor controls and power electronics.



**Mogens Lau** received the M.Sc. in Electrical engineering from Aalborg University, Aalborg, Denmark, in 1999. He worked as development engineer, project manager and line manager within power electronics at leading companies like Siemens, Danfoss, Grundfoss and Vestas. Currently, he is the working with Siemens Wind Power A/S in Brande, Denmark.